4-Hydroxyphenylpyruvate Dioxygenase: A Hybrid Density Functional Study of the Catalytic Reaction Mechanism

ARTICLE *in* BIOCHEMISTRY · OCTOBER 2004

Impact Factor: 3.02 · DOI: 10.1021/bi049503y · Source: PubMed

3 AUTHORS, INCLUDING:

Tomasz Borowski

Instytut Katalizy i Fizykochemii Powierzchni i…

45 PUBLICATIONS **1,219** CITATIONS

SEE PROFILE

4-Hydroxyphenylpyruvate Dioxygenase: A Hybrid Density Functional Study of the Catalytic Reaction Mechanism

Tomasz Borowski,* Arianna Bassan, and Per E. M. Siegbahn

Department of Physics, Stockholm Center for Physics, Astronomy, and Biotechnology, Stockholm University, S-106 91, Stockholm, Sweden

Received March 12, 2004; Revised Manuscript Received July 23, 2004

ABSTRACT: Density functional calculations using the B3LYP functional has been used to study the reaction mechanism of 4-hydroxyphenylpyruvate dioxygenase. The first part of the catalytic reaction, dioxygen activation, is found to have the same mechanism as in α-ketoglutarate-dependent enzymes; the ternary enzyme−substrate−dioxygen complex is first decarboxylated to the iron(II)-peracid intermediate, followed by heterolytic cleavage of the O−O bond yielding an iron(IV)-oxo species. This highly reactive intermediate attacks the aromatic ring at the C1 position and forms a radical σ complex, which can either form an arene oxide or undergo a C1−C2 side-chain migration. The arene oxide is found to have no catalytic relevance. The side-chain migration is a two-step process; the carbon−carbon bond cleavage first affords a biradical intermediate, followed by a decay of this species forming the new C−C bond. The ketone intermediate formed by a 1,2 shift of an acetic acid group rearomatizes either at the active site of the enzyme or in solution. The hypothetical oxidation of the aromatic ring at the C2 position was also studied to shed light on the 4-HPPD product specificity. In addition, the benzylic hydroxylation reaction, catalyzed by 4-hydroxymandelate synthase, was also studied. The results are in good agreement with the experimental findings.

α-Keto-acid-dependent dioxygenases constitute the largest family of mononuclear non-heme iron enzymes, and as a consequence of their abundance, representatives of this family are involved in many essential metabolic transformations (*1*−*8*). In most cases, these enzymes utilize 2-oxoglutarate (α-ketoglutarate, α-KG),[1] which plays the role of a cosubstrate binding to the iron(II) active site and delivering, through oxidative decarboxylation, two electrons necessary for dioxygen activation. However, for a small subfamily, comprising 4-hydroxyphenylpyruvate dioxygenase (4-HPPD) and 4-hydroxymandelate synthase (4-HMAS), the primary substrates possess an inbuilt α-keto acid functionality, which is used for dioxygen activation instead of the α-KG cosubstrate. The catalytic mechanism of these two internal keto-acid-dependent dioxygenases is the theme of the present theoretical report.

4-Hydroxyphenylpyruvate dioxygenase is involved in tyrosine catabolism and seems to be important for at least two reasons. First, a hereditary disease, tyrosinemia, is related to defective tyrosine degradation, and one type of this inborn defect of metabolism can be treated with 4-HPPD inhibitors (*9*, *10*). Second, the biosynthesis of plastoquinons and tocopherols, i.e., electron carriers and singlet oxygen scavengers essential for photosynthesis, depends on the 4-HPPD activity (*11*). Therefore, inhibition of 4-HPPD is a new mode of herbicidal action (*12*).

Like other α-keto-acid-dependent dioxygenases, 4-HPPD in the active form binds one ferrous ion per protein molecule (*13*). The physiological reaction of 4-HPPD involves keto acid decarboxylation, phenyl ring hydroxylation, and side-chain rearrangement (see Scheme 1). In other words, the pyruvic side chain is transformed into an acetic acid group, which migrates to the adjacent carbon of the ring, while the original position of the side-chain binding is hydroxylated. Similar to α-ketoglutarate-dependent dioxygenases, binding of substrates and product release is sequential. 4-Hydroxyphenylpyruvate (4-HPP) binds to the enzyme prior to dioxygen, while CO_2 is the first product released (*14*, *15*).

Quite recently, another internal keto-acid-dependent dioxygenase was identified. 4-Hydroxymandelate synthase (4-HMAS), which is involved in the biosynthesis of vancomycin antibiotics, is closely related to 4-HPPD. The two enzymes exhibit 43% sequence similarity and have the same substrate, i.e., 4-HPP (*16*). Furthermore, Townsend and co-workers recently obtained point mutants of 4-HPPD exhibiting 4-HMAS activity (*17*). 4-HMAS catalyzes the conversion of 4-HPP into 4-hydroxymandelate (4-HMA), i.e., the decarboxylation and benzylic hydroxylation of 4-HPP (see Scheme 1).

Isotope-labeling experiments performed for 4-HPPD and 4-HMAS indicate that one atom of dioxygen is incorporated into the carboxyl group of the product, while the second one is found in hydroxyl groups of homogentisate or 4-HMA (see Scheme 1). However, at least 50% of the oxygen at these hydroxyl groups originate from the solvent, which

* To whom correspondence should be addressed. Telephone: +46 8 55378703. Fax: +46 8 55378601. E-mail: borowski@physto.se.

[1] Abbreviations: 4-HPPD, 4-hydroxyphenylpyruvate dioxygenase; 4-HPP, 4-hydroxyphenylpyruvate; 4-HMAS, 4-hydroxymandelate synthase; 4-HMA, 4-hydroxymandelate; TauD, taurine/α-ketoglutarate dioxygenase; 4-HPA, 4-hydroxyphenylacetate; DFT, density functional theory; PES, potential-energy surface; α-KG, α-ketoglutarate; TS, transition state.

10.1021/bi049503y CCC: $27.50
Published on Web 08/28/2004

Scheme 1: Native Reactions Catalyzed by 4-HPPD and 4-HMAS[a]

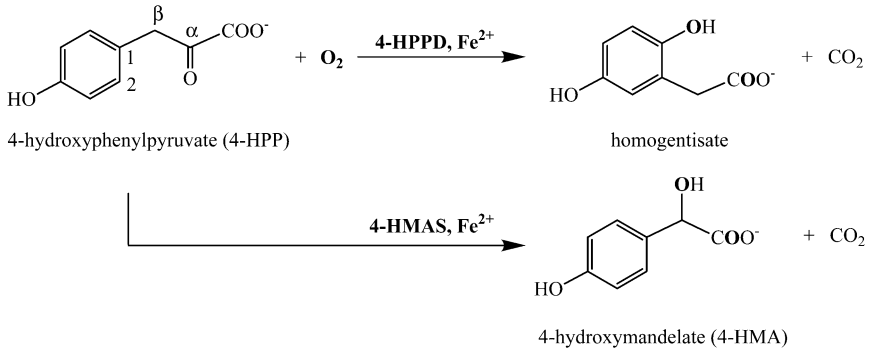

[a] In the products, atoms originating from dioxygen are bold.

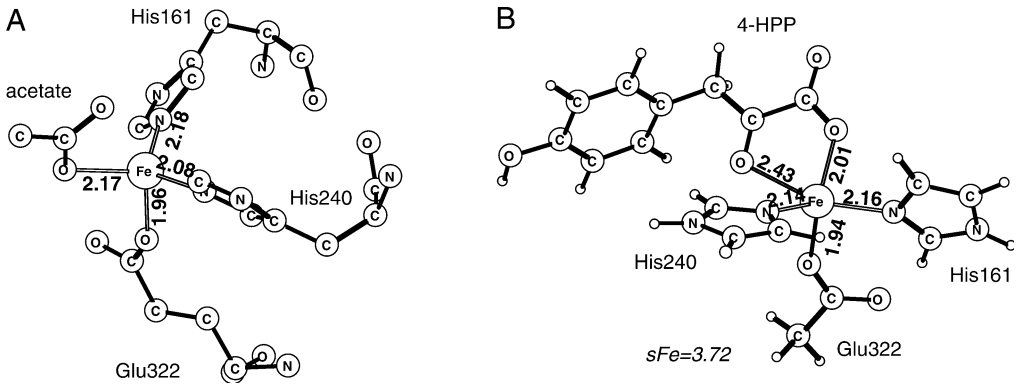

FIGURE 1: (A) Crystal structure of the 4-HPPD active site. (B) Computational model used in this study.

implies that some intermediate capable of exchanging oxygen with water is formed in the catalytic cycle of the two enzymes (*16*, *18*).

Up to now crystallographic information is available only for one internal α-keto-acid-dependent dioxygenase. In this 2.4 Å resolution structure of *Pseudomonas fluorescens* 4-HPPD (PDB access code 1CJX) (*19*), the active-site iron is in the ferric oxidation state and coordinated by the side chains of two histidines and one glutamate (His161, His240, and Glu322; see Figure 1). These ligands form a common iron-binding motif found in many mononuclear non-heme iron enzymes (*20*). The fourth coordination site of the Fe^{III} ion is occupied by acetate, which was present in the crystallization buffer, and the coordination geometry of the active-site iron is described as distorted tetrahedral. Even though the experimental structure of the enzyme−substrate complex is not available, 4-HPP was modeled into the active site (*19*). In this computational model exploiting the structural similarity between 4-HPPD and 2,3-dihydroxyphenyl dioxygenase, the α-keto acid group of 4-HPP replaces the buffer acetate and chelates the ferrous ion, while the sixth coordination site, which is unoccupied, is proposed to be the place of dioxygen binding.

A number of experimental observations pertaining to the chemistry carried out by 4-HPPD shed light on the catalytic mechanism of this enzyme. For example, it was established that acetic acid group shift occurs with the retention of configuration around the migrating carbon (Cβ in Scheme 1), while a proton, ortho to the acidic substituent, i.e., bound to the C2 carbon, is lost during the side-chain migration (*21*, *22*). Further aspects of the 4-HPPD chemistry were revealed in experiments with nonphysiological substrates. For example, rat liver 4-HPPD catalyzes aliphatic hydroxylation and sulfoxidation (*23*−*25*), which are typical reactions for heme-containing oxygenases (*26*). Therefore, a high-valent iron-oxo species, similar to compounds I and II in heme enzymes, was proposed to be the product of dioxygen activation in 4-HPPD. Interestingly, recent studies on taurine/α-ketoglutarate dioxygenase (TauD) have provided strong evidence for the catalytic relevance of such a high-spin iron-oxo species (*27*−*29*). In addition, the ability of mammalian liver 4-HPPD to oxidize fluoro and deoxy analogues of 4-HPP was interpreted as an indication that the 4-hydroxo group of 4-HPP is not absolutely necessary for the catalytic reaction (*30*). Finally, it was suggested that arene oxide could be an intermediate in the catalytic reaction because its formation is consistent with the identity of some observed, though usually abnormal, products (*31*). The recent studies by Townsend and co-workers showed that some point mutants of *Streptomyces avermitilis* 4-HPPD produce oxepinone, which is a product of arene oxide ring expansion and ketonization (*17*). On the other hand, there is also some experimental evidence against the catalytic intermediary of the arene oxide, because its analogue does not show the expected inhibitor activity (*32*). Considering the rate of the catalytic reaction, recent studies on 4-HPPD from *Streptomyces avermitilis* showed that an oxygenated intermediate, the identity of which is still to be determined, accumulates in turnover and decays at the catalytically relevant rate of 7.8 s^{-1} (*15*).

COMPUTATIONAL DETAILS

The computational model of the 4-HPPD active site was constructed from the crystal structure available (PDB access code 1CJX; see Figure 1). The protein ligands coordinating

to iron were modeled by imidazoles and acetate. The buffer acetate found in the crystal structure was replaced by the substrate, i.e., 4-HPP. Like in the structure proposed for the enzyme−substrate complex, 4-HPP binds to the ferrous ion opposite to the two histidines (*19*). The sixth coordination position, trans to glutamate, is unoccupied and this is the proposed dioxygen-binding site.

Because binding of 4-HPP most probably induces some geometry changes at the iron site, no constraints were imposed on the atomic coordinates of the model. Obviously, the model employed here cannot reproduce the steric field of the active-site pocket, hence the hydroxyphenyl side chain of 4-HPP moves considerably when going through structures of the stationary points for the first part of the catalytic reaction. However, while the range of these conformational changes is probably reduced in the active-site pocket, it is believed that these geometrical variations should hardly affect the energetics calculated. The possible significance of the active-site steric field for the reaction mechanism is addressed in the Results and Discussion.

Because of the fact that the crystal structure of 4-hydroxymandelate synthase is not yet available, the same model was employed in the study of the benzylic hydroxylation reaction. This approach seems to be justified by the 4-HPPD/4-HMAS sequence alignment indicating that the same ligands coordinate to iron in the two enzymes (*17*).

All calculations were performed employing hybrid Density Functional Theory (DFT) with the B3LYP (*33*, *34*) exchange-correlation functional. Two programs, Gaussian (*35*) and Jaguar (*36*), were used. Geometry optimizations were performed with a valence double-ζ basis set coupled with an effective core potential describing the innermost electrons on iron. This particular basis set is labeled lacvp in Jaguar. For the optimized structures, the electronic energy was computed with a bigger basis set of triple-ζ quality with polarization functions on all atoms (labeled lacv3p** in Jaguar). The solvent corrections were calculated with the self-consistent reaction-field method implemented in Jaguar (*37*, *38*). A dielectric constant of 4 with a probe radius of 2.50 Å was used to model the protein surrounding the active site, while values of 80.4 and 1.40 Å were used for modeling the enolization reaction in water. Although the actual dielectric constant of the protein might be somewhat different from the chosen value, it should be stressed that the dielectric energy effects depend on the dielectric constant as $(\epsilon - 1)/\epsilon$. Therefore, the energetic effect of changing the constant between 1.0 and 4.0 is much larger than changing it between 4.0 and, for example, 20.0. Because the dielectric effects using $\epsilon = 4.0$ are quite small for the present reaction, using a different but feasible value of the dielectric constant would hardly change the calculated energetics.

Because in several intermediates found in this study (e.g., quintet σ complexes and quintet biradical and benzylic radical species), spins on various parts of the complexes are antiferromagentically coupled, a spin correction to the energy of these species was calculated using the broken symmetry approach (*39*, *40*). The recommended strong localized limit was assumed, which means a zero overlap between the magnetic orbitals (*40*). This specific computational methodology has successfully been applied to a wide range of redox enzymes with transition metals at their active sites (*41*−*43*). The energies reported are relative values calculated with respect to the isolated reactants, i.e., the 4-HPP active-site complex and dioxygen.

RESULTS AND DISCUSSION

Presently, there seems to be a consensus that the first part of the catalytic reaction of 4-HPPD and 4-HMAS, i.e., the dioxygen activation, proceeds in the same way as in α-KG-dependent enzymes (*2*, *3*, *7*, *8*). Because the results reported here confirm this opinion and α-KG-dependent enzymes have been examined by means of a similar computational approach in a previous study (*44*), the oxidative decarboxylation of 4-HPP is only briefly addressed here. Instead, the major emphasis of the discussion is put on the further catalytic steps of 4-HPPD, i.e., phenyl ring oxidation, side-chain migration, and rearomatization. The intermediates involved in the suggested 4-HPPD catalytic cycle and the possible side reactions are presented in Scheme 2, which is intended to aid with the reading of this section.

Two mechanisms concerning the aromatic ring oxidation catalyzed by 4-HPPD have recently been proposed (see Scheme 3) (*3*, *31*).

In one of them, involving species **5**, **I**, **9**, **II**, and **8**, it was suggested that the iron(IV)-oxo group attacks the phenyl ring of the substrate yielding an intermediate with a four-membered ring comprising an Fe−C bond (**I**) (*31*). Then, **I** rearranges to the arene oxide intermediate (**9**), which subsequently opens the epoxide ring forming the cation σ complex (**II**). The 1,2 shift of the acetic acid side chain transforms **II** into the ketone intermediate (**8**), which rearomatizes to the final product, homogentisate, either in the active site of 4-HPPD or in solution. In the second mechanism, comprising intermediates **5**, **II**, and **8**, the iron-(IV)-oxo species (**5**) performs an electrophilic attack on the C1 carbon atom of the phenyl ring, which directly affords **II** (*3*). Further catalytic steps, which lead from **II** to the final product, homogentisate, coincide for the two proposed mechanisms.

This paper reports the results of a computational study undertaken with the aim of improving our understanding of the 4-HPPD catalytic reaction mechanism. More specifically, the answers for the following mechanistic questions were pursued: (1) Is the organo-iron intermediate (**I**) feasible? (2) What is the origin of the product specificity? (3) Is **9** an obligatory intermediate in the enzymatic reaction? (4) Does the rearomatization reaction proceed in the active site or in solution? The results reported here provide some clues concerning these issues.

Dioxygen Activation in 4-HPPD and 4-HMAS. The calculated potential-energy surface (PES) for dioxygen activation in 4-HPPD and 4-HMAS is shown in Figure 2. The starting point for the reaction is the five-coordinated (5C) iron site with a bound substrate. The vacancy in the iron coordination shell was previously shown to be of crucial importance for the rate of the biomimetic reaction, and it was also proposed that in α-KG-dependent enzymes the 5C iron center must be available for O_2 binding (*5*, *45*, *46*). Even though the trapping of dioxygen by the 5C site is calculated to be thermodynamically unfavorable (by 6.3 and 3.8 kcal/mol for the quintet and septet states, respectively), the quintet Fe−O_2 species (**2**) needs to be formed for the reaction to continue. The electronic structure of this adduct is best

Scheme 2: Suggested Mechanism of the 4-HPPD Catalytic Cycle and Possible Side Reactions

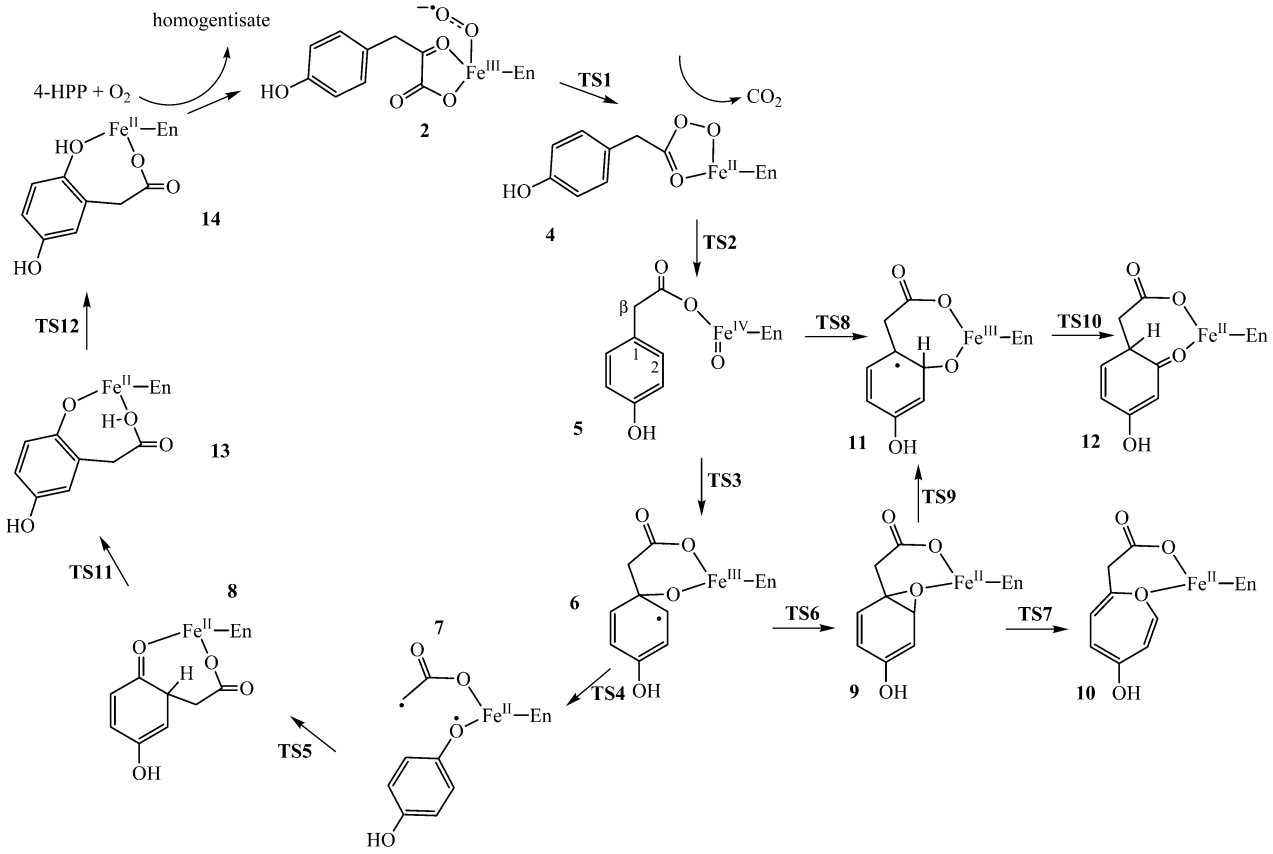

described as $Fe^{III}-O_2^{-}\bullet$. It is the superoxo character of the bound dioxygen together with the fact that the next intermediate has a quintet ground state that make the quintet PES optimal for the initial 2-electron reduction of dioxygen. The transition state **TS1**, presented in Figure 3A, connects the quintet iron-dioxygen species (**2**) with the iron(II)-peracid complex (**3**), in which a CO_2 molecule is very loosely bound to iron. Therefore, it is concluded that CO_2 is released from the active site at this stage of the catalytic cycle, which is in accordance with the ordered Bi Bi kinetic mechanism proposed for human liver 4-HPPD, where CO_2 is the first product released (*14*).

The final step of oxygen activation is the heterolytic cleavage of the O−O bond in the Fe^{II}-peracid species (**4**). This elementary reaction, which leads to **5** and involves a low activation barrier (5.0 kcal/mol), can be viewed as a two-electron reduction of the peracid at the expense of ferrous ion. The structures of the transition state **TS2** and the product of this step are presented in Figures 3B and 4, respectively. On the septet PES, the dioxygen activation is a one-step process. However, the septet transition state for concerted O−O bond cleavage and α-keto acid decarboxylation lies 8.2 kcal/mol above the quintet **TS1**, which means that the septet path is most likely not used by the enzyme.

It is interesting to note here that a very similar two-step mechanism on the quintet PES was previously found for tetrahydrobiopterin-dependent amino acid hydroxylases (*47*). Also in this case, the first 2-electron reduction of O_2 was found to be the rate-limiting step, leading to the peroxo-bridged structure, which subsequently undergoes a heterolytic O−O bond cleavage. α-Keto-acid-dependent dioxygen activation yields the iron(IV)-oxo species, which is a powerful oxidant used in the subsequent catalytic steps. This species has three close lying spin states: the ground state quintet and the triplet and septet states lying 3.6 and 12.5 kcal/mol above it, respectively (see Figure 2).

Scheme 3: Mechanisms Proposed for the Second Part of the 4-HPPD Catalytic Reaction which Involves the Phenyl Ring Oxidation (En = Enzyme)

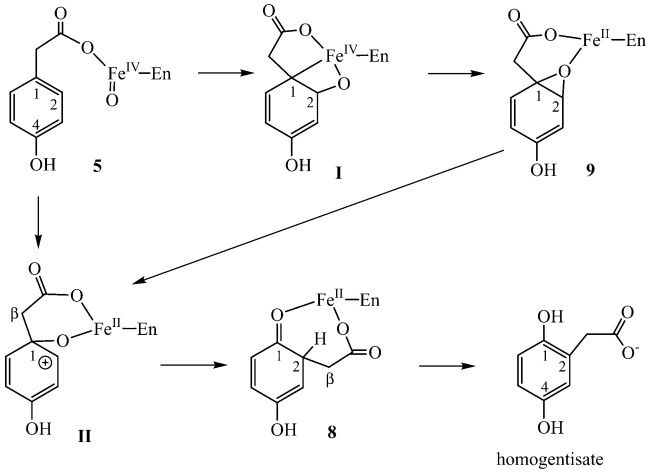

Attack of the Activated Oxygen Species on the Phenyl Ring. The relative energies calculated for 4-HPPD **5** indicate that all three spin states could in principle be involved in an electrophilic attack on the phenyl ring. However, the previously calculated barrier heights for the biomimetic complex indicate that only the quintet and septet PES need to be explored for the initial step of the aromatic ring oxidation (*48*).

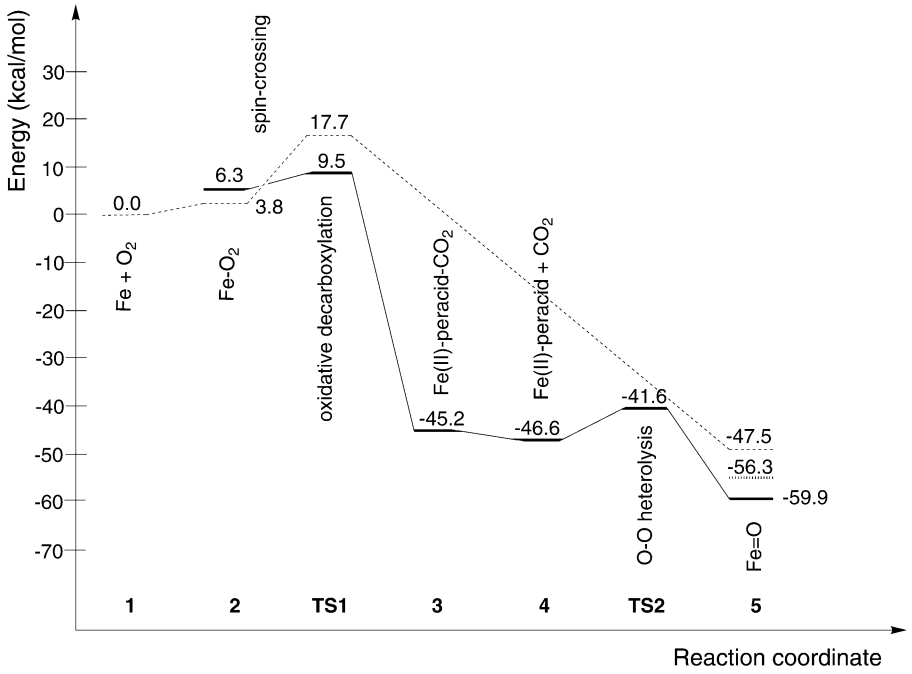

FIGURE 2: PES for the dioxygen activation part of the 4-HPPD and 4-HMAS catalytic cycle, with the quintet (solid line), septet (dashed line), and triplet (hashed line) spin states. The bold labels correspond to the quintet species and the septet spin state of the separate reactants (**1**).

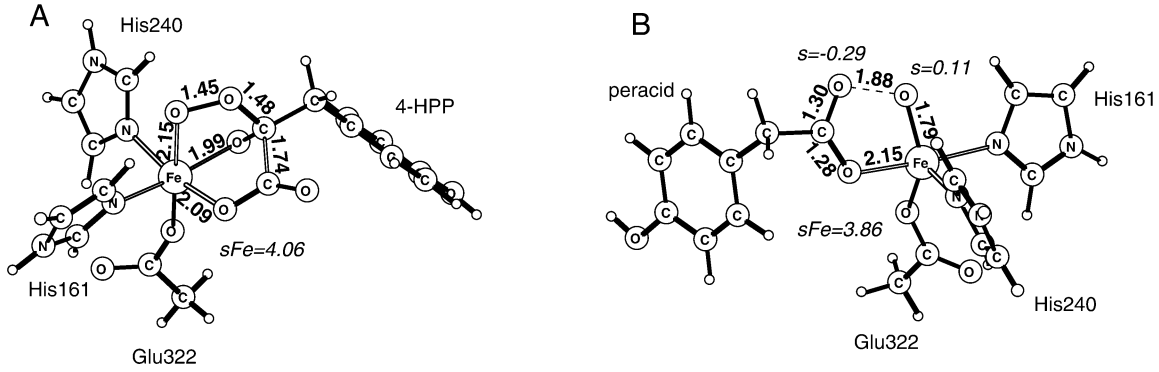

FIGURE 3: (A) **TS1**, the transition state for the 4-HPP decarboxylation reaction. (B) **TS2**, the transition state for the O−O heterolysis.

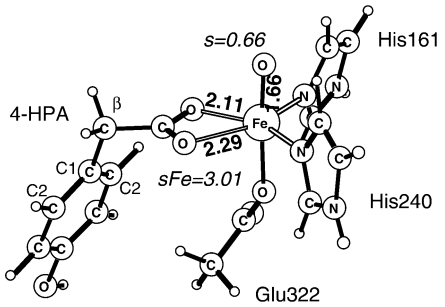

FIGURE 4: **5**, the iron(IV)-oxo intermediate in the quintet ground state.

The calculated energy diagram for the 4-HPPD phenyl ring oxidation reaction is presented in Figure 5. The reaction starts with an electrophilic attack of **5** on the C1 carbon of the phenyl ring, which leads through **TS3** to the radical σ complex (**6**; see Figure 6). The calculated activation barrier for the quintet PES (16.9 kcal/mol) compares favorably with the barriers reported previously for the α-KG biomimetic system (14.9 kcal/mol) (*48*) and the phenylalanine hydroxylase (16.2 kcal/mol) (*49*). The septet transition state for this reaction lies 5.7 kcal/mol above **TS3**, while the product, i.e., the septet radical σ complex, has a very similar energy and spin distribution as the quintet species (**6**). The formation of an Fe^{III}-radical (**6**) rather than an Fe^{II}-arenium cation σ complex (**II**) can be attributed to the presence of two negatively charged ligands in the iron coordination shell. Indeed, in the previous study, it was found that two anionic ligands stabilize the ferric state and hinder the transfer of the second electron from the ring to iron (*49*). A similar behavior was also observed for the biomimetic complex (*48*).

Notably, the alternative mechanisms for the aromatic ring activation were ruled out. First, the intermediate with an iron−carbon bond (**I**; see Scheme 3) is not stable. During the geometry optimization of this species, the iron−carbon bond breaks and the structure converges to the C2 radical σ complex (**11**), which could be formed in an electrophilic attack of the iron-oxo species on the C2 carbon. Furthermore, the energy calculated for the optimized structure (constrained optimization) with an iron−carbon bond length of 1.9 Å is 32.3 kcal/mol higher than that for optimized **11**. Second, the

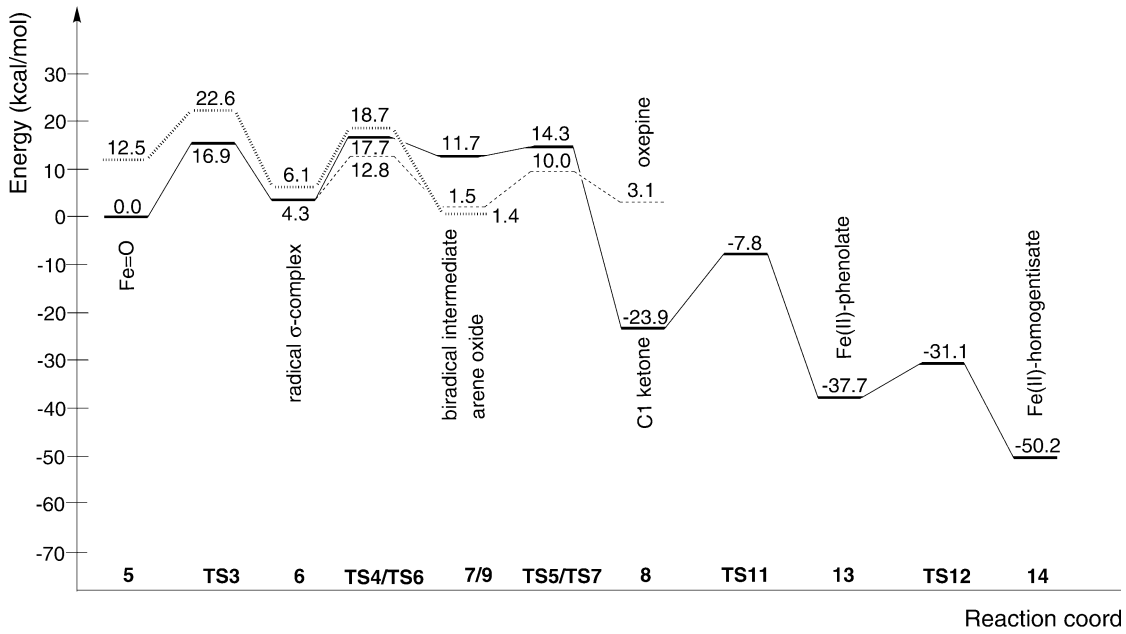

FIGURE 5: PES for the aromatic ring oxidation part of the 4-HPPD catalytic cycle, with the reaction pathway following the electrophilic attack on the C1 carbon (quintet PES; solid line), the arene oxide side reaction (quintet PES; dashed line), and the septet electrophilic attack on the C1 carbon and the subsequent C1−Cβ bond cleavage (hashed line). The bold labels correspond to the quintet species only.

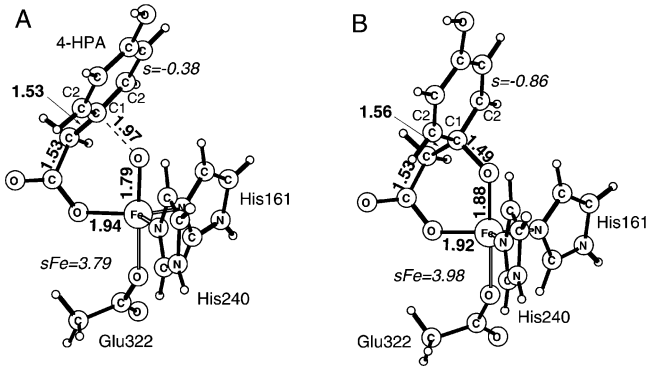

FIGURE 6: (A) **TS3**, the transition state for the electrophilic attack of the iron-oxo species on the C1 carbon. (B) **6**, the radical C1 σ complex in the quintet ground state.

direct formation of **9** from **5** was also found to be energetically unfavorable. In a series of restrained optimizations, where the C1−O and C2−O bond lengths were kept equal, an approximate stationary point leading from **5** to **9** was localized. However, the energy calculated for this geometry is high (25.7 kcal/mol with respect to **5**), and the frequency analysis indicates that it is not a transition state but rather a second-order saddle point characterized by two imaginary frequencies. Like in the computational study on ethane epoxidation by cytochrome P-450 (*50*), one frequency corresponds to the symmetrical oxygen insertion into the double bond, while the second one leads to the ordinary transition states for the electrophilic attack on either of the two carbon atoms. Therefore, the reaction coordinate for symmetric oxygen-atom insertion does not lie on the minimum energy path. This conclusion is strongly corroborated by the results of previous theoretical studies dedicated to the arene and olefin oxidation by high-valent iron-oxo species (*49*−*54*).

Acetic Acid Side-Chain Migration. The 100% efficient 1,2 shift of the relatively large side chain is a fascinating feature unique to the 4-HPPD activity. Analogous 1,2 rearrangements, usually inferred to as NIH shifts, are observed for other aromatic ring oxidizing enzymes, though the migrating group is usually a hydrogen atom and the efficiency of the rearrangement is usually lower than 100% (*26*, *55*−*59*). Therefore, this reaction is one of the most intriguing parts of the 4-HPPD catalytic cycle.

In regards to the prerequisites for this rearrangement, it is interesting to note that both mechanisms, shown in Scheme 3, assume that the alkyl-chain migration takes place in **II** and not in **9**. The computational results are consistent with this proposal, because the direct migration of the side chain in **9** was found untenable. In this and previous theoretical studies, all attempts to find a transition state connecting **9** with **8** gave very steep energy increases along the approximate reaction coordinates (*49*, *51*).

As for the mechanism of the rearrangement, it was found that this reaction consists of two elementary steps connected by an unstable biradical species (**7**; see Scheme 4). First, the C1−Cβ bond cleaves leading through **TS4** to **7** (see Figure 7). Because it turns out that this **TS4** is the highest energy point along the pathway for the productive decay of **5**, the calculated accumulated barrier for this process is 17.7 kcal/mol. This value compares well with the 15.1 kcal/mol barrier estimated from the decay rate of an oxidized intermediate recently observed in *Streptomyces avermitilis* 4-HPPD (*15*). In **7**, spins on the fragments that are supposed to make a new bond are of opposite sign, which suggests that the next catalytic step should be very easy. Indeed, the calculated activation energy for the rebound process at the C2 position (**TS5**) is only 2.6 kcal/mol.

The low activation barrier for the decay of the biradical intermediate is in line with the experimental observation that the side chain migrates with retention of configuration (*21*). In the carboxy-methyl radical, the calculated barrier for rotation around the C−C bond is 8.6 kcal/mol, which is substantially higher than the barrier for the rebound process, and hence, the racemization at the Cβ carbon does not take place. Interatomic distances and spin populations reported

Scheme 4: Two Mechanisms for the NIH shift in the 4-HPPD Reaction: (A) Two-Step Mechanism Found in this Study and (B) Carbocation Mechanism (En = Enzyme)

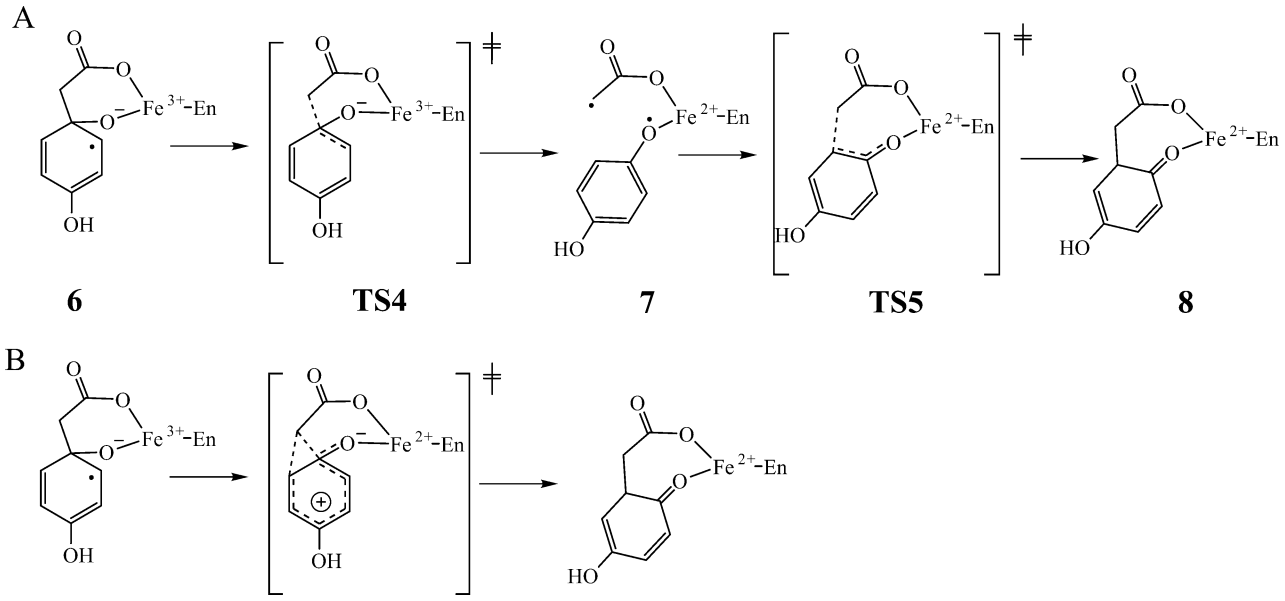

for **TS5** in Figure 8A are consistent with the rebound mechanism for the side-chain migration; the spin populations on the carbons forming the new bond are of opposite sign, while the distance between the migrating carbon (Cβ) and the C2 position (2.75 Å) is smaller than the C1−Cβ separation (3.17 Å). Moreover, the Hessian calculations show that there is only one imaginary frequency, and it corresponds to the reaction coordinate describing the C2−Cβ bond formation.

On the septet PES, the cleavage of the C1−Cβ bond proceeds in an analogous way as on the quintet PES (for energetics, see the hashed line of Figure 5). However, even though the septet biradical species was found 10.3 kcal/mol more stable than **7**, it must be stressed that the catalytic reaction cannot continue on the septet PES. The reason is that, to form the Cβ−C2 bond, antiparallel spins on the two fragments are necessary, while in the septet species, all open-shell electrons have parallel spins. Therefore, it is concluded that if the septet species are formed, they have to be (de)-excited into the quintet PES so that the enzymatic process can continue.

Arene Oxide Side Reaction. The results reported in the two previous subsections show that **9** (Scheme 2) can neither be formed directly from **5** nor is it a necessary intermediate for the NIH shift. Therefore, **9** is not a catalytic cycle intermediate. Notably, a similar conclusion was previously drawn from experimental and theoretical studies on other enzymes proposed to utilize the high-valent iron-oxo complex for oxidizing aromatic rings (*49*, *51*, *55*, *57*). Nevertheless, the formation and possible reactions of **9** were investigated, first, because there is strong evidence for the presence of this species among the products of some 4-HPPD point mutants (*17*) and, second, to gain a full picture of the chemistry performed by this interesting enzyme.

The epoxide ring of **9** is formed by constituting a bond (**TS6**) between the oxygen atom and the C2 carbon in **6**. This process is relatively easy, because it involves the lowest barrier available for **6** (8.5 kcal/mol; see Figure 5). Once **9** is formed, the reaction can continue in three directions. First,

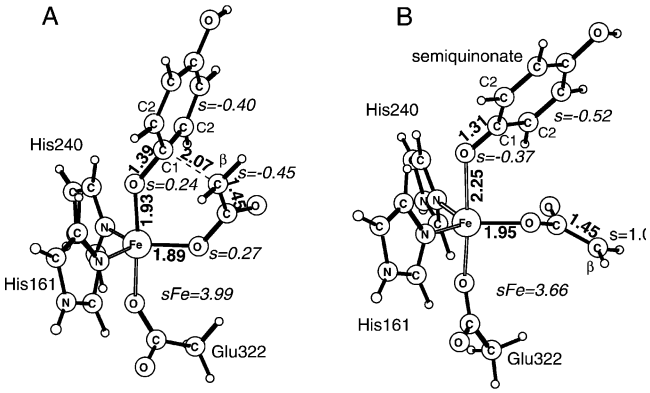

FIGURE 7: (A) **TS4**, the first transition state for the side-chain migration, C1−Cβ bond cleavage. (B) **7**, the biradical intermediate formed during the side-chain shift.

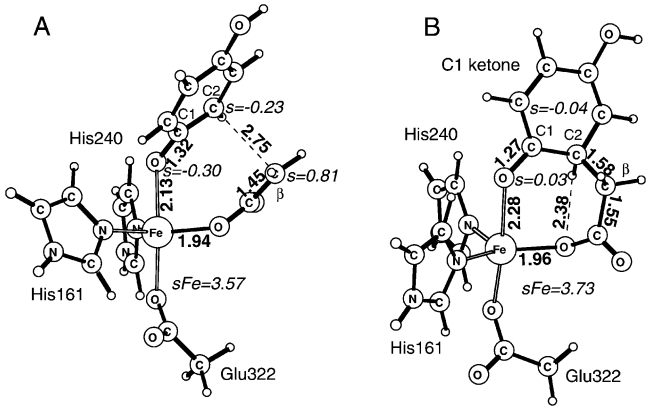

FIGURE 8: (A) **TS5**, the second transition state for the side-chain migration, C2−Cβ bond formation. (B) **8**, the product of the side-chain migration, the C1 ketone intermediate.

the cleavage of the C2−O bond can restore **6**. Second, the cleavage of the other epoxide bond, C1−O, affords a different radical, now **11**. The consequences and energetics of this reaction are discussed in the next subsection. Finally, the third bond in the epoxide ring, C1−C2, can also be cleaved (**TS7**), and this reaction yields an oxepine species

(**10**). This reaction involves a barrier of the same size as that for the arene oxide formation (8.5 kcal/mol), and it is a reversible reaction because its energy is only 1.6 kcal/mol.

In summary, the energetics obtained for the arene oxide branch of the 4-HPPD catalytic cycle indicate that **6** may exist in equilibrium with **9** and **10**. Although these species are not directly involved in the main catalytic reaction of 4-HPPD, they might be produced and released to solution by mutated forms of the enzyme, which lack the native product specificity (*17*, *60*).

C2 Path and 4-HPPD Product Specificity. One of the intriguing aspects of enzymatic catalysis is the high product specificity usually exhibited by enzymes. In the case of 4-HPPD, it is manifested by the fact that only homogentisate is produced by the native enzyme, while other possible products, like arene oxide or products of hydroxylation at positions other then C1, are normally not observed. When the fact that the observed 4-HPPD product selectivity most likely results from an intricate interplay of various factors was recognized, the contribution from the electronic and geometrical structure of the iron site was investigated as a part of this study. With this aim in mind, two possible branching points on the PES, which might lead to products different from homogentisate, were analyzed. First, the electrophilic attack of **5** at the C1 and C2 carbons of various substrates was studied to check if any of these two adjacent sites is preferred. Second, the reaction initiated either by the C1−O bond cleavage in **9** or by the electrophilic attack at the C2 carbon of 4-hydroxyphenylacetate (4-HPA) and leading to the C2-hydroxylated product was investigated. The results of this analysis, reported in this subsection, provide insight into the factors affecting the 4-HPPD product specificity.

5 produced in the first part of the 4-HPPD catalytic cycle is a highly reactive intermediate, which performs the electrophilic attack on the C1 carbon of 4-HPA. Because no other positions in the aromatic ring are hydroxylated, the question of mechanistic importance is why the C1 carbon is favored. Although there are three alternative sites of the aromatic ring hydroxylation, in the present study, only the C2 position was taken into account. This particular choice seems to be justified by the following facts. First, the C2 carbon is the nearest one to the C1 position, and therefore, the geometrical structures of the intermediates resulting from an attack at these two sites should not be very different. This, in turn, should minimize the difference of the steric effects exerted by the protein envelope. Second, there is an experimental precedence for the oxidation at the C2 position in the case of 3-thienylpyruvate. Finally, **11**, which is the product of the electrophilic attack at the C2 carbon, can also be produced by the C1−O bond cleavage in **9**. This last species was indirectly observed for some point mutants of 4-HPPD (*17*).

Considering the first possible branching point, the transition states for electrophilic attacks at the C1 and C2 carbons in four 4-HPPD substrates having different aromatic rings were optimized, and the calculated activation energies are gathered in Table 1. In addition to the physiological substrate, 4-HPP, phenylpyruvare, 4-fluorophenylpyruvate, and 3-thienylpyruvate were taken into account. From the data reported in Table 1, it follows that the activation energy for the attack at the C2 carbon in 4-HPA is 2.8 kcal/mol higher than that in the case of the C1 carbon. This activation energy difference can be used to estimate the expected concentration ratio of the C1 and C2 products. At room temperature, the C1/C2 ratio amounts to 113:1, which shows that already the relatively small model used in this study correctly predicts the preferred position of hydroxylation. Moreover, the calculations performed for other substrates of 4-HPPD also properly predict the favored site of the electrophilic attack, i.e., 4-fluorophenylpyruvate is oxidized at the C1 position, while 3-thienylpyruvate is predicted to react at the C2 site much easier than at the C1 site. It can be noticed that only phenylpyruvate has a low activation energy difference, but it is currently not known if, for this substrate, the side chain migrates, the C2 position is directly hydroxylated, or both of these pathways are used by the enzyme. Most importantly, however, the difference in the calculated barriers for attacks at C1 and C2 carbons is sufficient to explain the identity of the products derived from the four substrates. The calculated C1/C2 product ratio is in all cases in favor of the actual product observed experimentally.

Table 1: Calculated Activation Energies [kcal/mol] for Electrophilic Attack at the C1 and C2 Positions of 4-HPPD Substrates Possessing Different Aryl Rings[a]

ring type	C1 $\Delta E^{\ddagger}$	C2 $\Delta E^{\ddagger}$	$\Delta\Delta E^{\ddagger}$	C1/C2 product ratio
4-hydroxyphenyl	16.9	19.7	2.8	113:1
phenyl	18.8	19.3	0.5	2.3:1
4-fluorophenyl	18.0	20.0	2.0	29:1
3-thienyl	18.0	15.1	−2.9	1:143

[a]Activation energy difference is used to calculate the product distribution at room temperature.

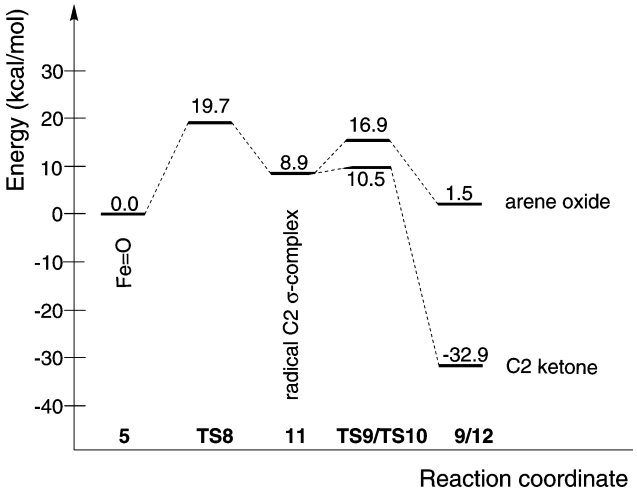

FIGURE 9: PES for the hypothetical reaction following the electrophilic attack of the iron(IV)-oxo species on the C2 carbon.

In regards to the second possible branching point, from Figure 9, it follows that the activation energy associated with the C1−O bond cleavage in the arene oxide (**9** → **11**) is 15.4 kcal/mol, while from the comparison of Figures 5 and 9, it is clear that **11** is 4.6 kcal/mol less stable than **6**. Although the calculated activation energy for the C1−O bond cleavage is higher than that for the analogous process involving the C2−O bond (**9** → **6**; 11.3 kcal/mol), the energy of this transition state (**TS9**) calculated with respect to **5** is comparable with the activation energy for the productive decay of **6** (16.9 versus 17.7 kcal/mol). This means that under steady-state conditions some fraction of **9** may open the

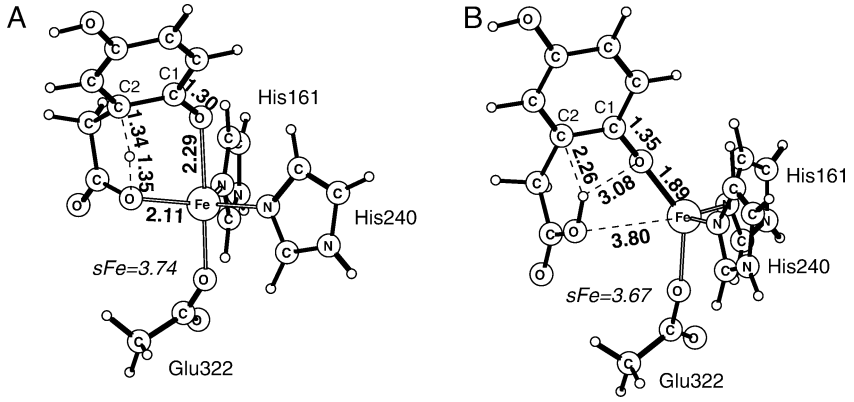

FIGURE 10: (A) **TS11**, the first transition state for the proton transfer in the ketone intermediate rearomatization. (B) **13**, the phenolate intermediate formed during the rearomatization process.

Scheme 5: Energetics of the Rearomatization Reaction Calculated for the Ketone Intermediate Released from the 4-HPPD Active Site

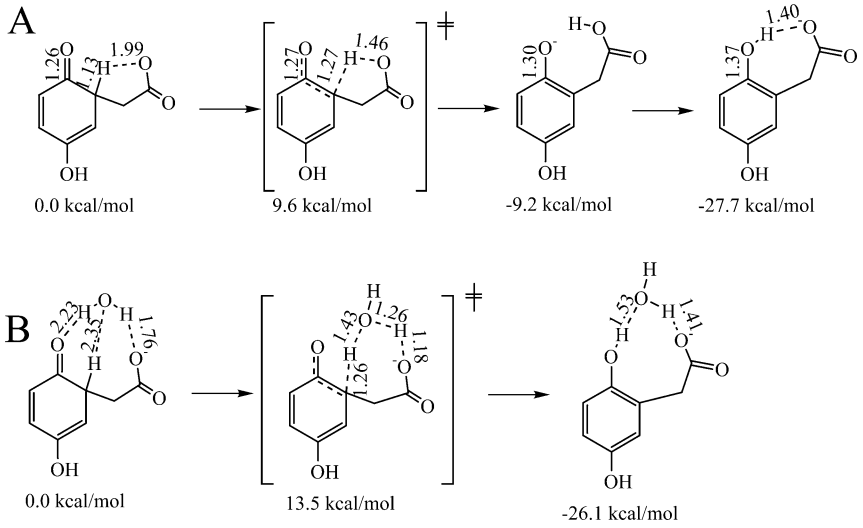

epoxide ring and form **11**. However, this process would be practically irreversible because the latter complex very readily undergoes an irreversible hydride NIH shift leading to the C2 ketone (**12**). Thus, to maintain the observed product specificity of 4-HPPD, in the real enzyme, the formation of **9** and/or its opening to **11** should be slightly more difficult, by a few kcal/mol, than that in the computational model employed here. For example, in light of the fact that **11** is more bulky than **6** (they have six- and seven-membered rings comprising iron, respectively), it seems reasonable to speculate that the steric strain of the protein could contribute a few kcal/mol to the barrier height for the transformation of **9** to **11**. Of course, this kind of steric interaction destabilizing **11** with respect to **6** would also increase the difference of the activation energies for the direct electrophilic attacks at these positions of 4-HPA. As a result, the productive decay of **6** would be faster than the formation of **11**, and the observed 4-HPPD product selectivity would be maintained.

In summary, the results discussed in this subsection indicate that the electronic effects are at least partially responsible for the observed product specificity of 4-HPPD. While the activation energy differences calculated for the direct electrophilic attack at the ring are sufficient to explain the preference in the oxidation position, it is proposed that some steric interaction between the residues lining the active-site pocket and **9** should disfavor the C1−O bond cleavage in the epoxide ring. This interaction, of a few kcal/mol, should guarantee that only homogentisate is produced in the enzymatic process.

Rearomatization Reaction. The final step in the transformation of 4-HPP to homogentisate is the enolization of **8**, which means a proton transfer from the C2 carbon to the ketone oxygen. In principle, because the ferrous oxidation state of the active-site iron is restored at this stage of the catalytic cycle, this tautomerization reaction can occur either at the active site of 4-HPPD or in solution. Interestingly, the computational results indicate that the rearomatization process can efficiently take place in any environment because the acetic acid side chain facilitates the proton transfer. In the first step, the proton bound to C2 is transferred to the carboxyl oxygen of the side chain (see Figure 10 and Scheme 5). This step involves a barrier of 16.1 and 9.6 kcal/mol at the active site (**TS11**) and in solution, respectively. Therefore, even though the barrier in the active site is considerable, it is still smaller than that for the rate-limiting step. Once the proton is transferred to the carboxyl group (**13**), the ring regains an aromatic character and the keto oxygen becomes a basic phenolic one. Thus, the transfer of the proton from the carboxyl group to the phenolic oxygen is an easy and exothermic process (at the active site, $\Delta E^{\ddagger} = 6.6$ kcal/mol; for structures of **TS12** and **14**, see Figure 11). Additional calculations performed for a model, where a water molecule

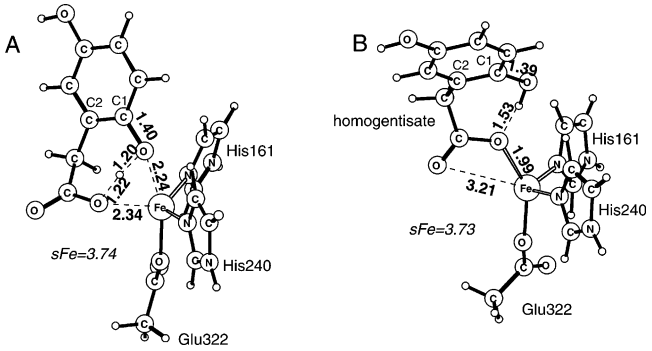

FIGURE 11: (A) **TS12**, the second transition state in the rearomatization reaction. (B) **14**, the final homogentisate-active-site complex.

mediates a proton transfer, showed that the solvent does not catalyze this reaction; i.e., the barrier is higher than that for the direct proton transfer (see Scheme 5).

In conclusion, the rearomatization reaction was found to proceed most easily in solution, but the activation barrier calculated for the active-site model is not prohibitively high, either. Therefore, the kinetics of **8** dissociation should control the actual place of rearomatization.

HMAS Activity: Benzylic Hydroxylation. The high sequence similarity between 4-HPPD and 4-HMAS along with the fact that some point mutants of 4-HPPD exhibit 4-HMAS activity support the assumption that both enzymes have similar iron-binding sites (*17*). After this, the reaction mechanism for benzylic hydroxylation was studied with the same model as the 4-HPPD catalytic cycle. While a full account of this study can be found in the Supporting Information, here, we only note that the 4-HMAS catalytic reaction involves a 15.4 kcal/mol barrier for the rate-limiting step, which is similar to the value of 17.7 kcal/mol found for the 4-HPPD reaction. Therefore, it is concluded that the precise orientation of the reactant, 4-HPA, at the active site controls the product specificity of these enzymes. Indeed, a single-point mutation of an amino acid located close to the iron-binding site was reported to spoil the product specificity of 4-HPPD, because apart from homogentisate, 4-hydroxymandelic acid and oxepinone were also produced by the 4-HPPD point mutants (*17*).

CONCLUSIONS

In the work reported here, the catalytic reaction mechanism of 4-HPPD was studied by means of the hybrid DFT. In summary, it was found that the decay of **5** is the rate-limiting step in the catalytic cycle. The calculated barrier for this reaction agrees well with the available experimental kinetics data. Interestingly, the acetic acid side-chain migration, which is unique to the 4-HPPD reaction, turned out to be a two-step process involving **7**. A fast productive decay of this species guarantees that the configuration around the migrating carbon is retained. Furthermore, the computational results strongly suggest that **9** is not a necessary intermediate in the reaction leading to homogentisate. The final rearomatization reaction was found to proceed with efficient rates both at the 4-HPPD active site and in solution. In addition, the product specificity of 4-HPPD is proposed to rely, at least partially, on the difference between activation barriers leading to **6** and **11**. The difference found for the electrophilic attack of the iron(IV)-oxo species on the aromatic ring would be sufficient to explain the selectivity, if the barrier for the opening of **9**, which leads to **11**, would be slightly increased (by a few kcal/mol) by the steric field of the active-site pocket. Finally, for the 4-HMAS activity, it was found that the first step, i.e., the Cβ−H bond cleavage, is rate-limiting. In conclusion, it is believed that the results reported here have clarified some issues concerning the 4-HPPD/4-HMAS catalytic mechanisms and may stimulate further experimental and theoretical studies on these interesting enzymes.

SUPPORTING INFORMATION AVAILABLE

Short summary of the previous computational results for the dioxygen activation in α-KG-dependent enzymes and their biomimetic system; short summary of the previous computational results for the electrophilic attack of the iron-oxo species on the phenyl ring in the biomimetic complex; results and discussion pertaining to the 4-HMAS catalytic reaction; table reporting the relative energies, Fe−O distances, and spin distributions for the three spin species of the iron-oxo intermediate; Scheme S1 presenting the suggested reaction mechanisms involving arene oxide; Scheme S2 with the reactions catalyzed by 4-HPPD involving deoxy and fluoro derivatives of 4-HPP; Scheme S3 showing the two possible reaction channels originating from two modes of the epoxide ring opening; Figure S2 presenting the structure of **9** and **TS6**; Figure S3 showing **10** and **TS7**; Figure S4 presenting the structure of **11** and **TS8**; Figure S5 showing the structure of the transition states for the transformation of the C2 σ complex to the arene oxide (**TS9**) and for the NIH shift in the C2 σ complex (**TS10**); Figure S6 presenting the structure of **12**; Figure S7 showing the structures of two transition states involved in the 4-HMAS catalytic reaction. This material is available free of charge via the Internet at http://pubs.acs.org.

REFERENCES

1. Prescott, A. G., and Lloyd, M. D. (2000) The iron(II) and 2-oxoacid-dependent dioxygenases and their role in metabolism, *Nat. Prod. Rep. 17*, 367−383.
2. Costas, M., Mehn, M. P., Jensen, M. P., and Que, L., Jr. (2004) Dioxygen activation at mononuclear nonheme iron active sites: Enzymes, models, and intermediates, *Chem. Rev. 104*, 939−986.
3. Bugg, T. D. H. (2003) Dioxygenase enzymes: Catalytic mechanisms and chemical models, *Tetrahedron 59*, 7075−7101.
4. Ryle, M. J., and Hausinger, R. P. (2002) Non-heme iron oxygenases, *Curr. Opin. Chem. Biol. 6*, 193−201.
5. Solomon, E. S., Brunold, T. C., Davis, M. I., Kemsley, J. N., Lee, S. K., Lehnert, N., Neese, F., Skulan, A. J., Yang, Y. S., and Zhou, J. (2000) Geometric and electronic structure/function correlations in non-heme iron enzymes, *Chem. Rev. 100*, 235−349.
6. Lange, S. J., and Que, L., Jr. (1998) Oxygen activating nonheme iron enzymes, *Curr. Opin. Chem. Biol. 2*, 159−172.
7. Que, L., Jr., and Ho, R. Y. N. (1996) Dioxygen activation by enzymes with mononuclear non-heme iron active sites, *Chem. Rev. 96*, 2607−2624.
8. Feig, A. L., and Lippard, S. J. (1994) Reactions of non-heme iron-(II) centers with dioxygen in biology and chemistry, *Chem. Rev. 94*, 759−805.
9. Tomoeda, K., Awata, H., Matsuura, T., Matsuda, I., Ploechl, E., Milovac, T., Boneh, A., Scott, C. R., Danks, D. M., and Endo, F. (2000) Mutations in the 4-hydroxyphenylpyruvic acid dioxygenase gene are responsible for tyrosinemia type III and Hawkinsinuria, *Mol. Genet. Metab. 71*, 506−510.

10. Lindstedt, S., Holme, E., Lock, E. A., Hjalmarson, O., and Strandvik, B. (1992) Treatment of hereditary tyrosinaemia type I by inhibition of 4-hydroxyphenylpyruvate dioxygenase, *Lancet 340*, 813−817.
11. Trebst, A., Depka, B., and Holländer-Czytko, H. (2002) A specific role for tocopherol and of chemical singlet oxygen quenchers in the maintenance of photosystem II structure and function in *Chlamydomonas reinhardtii*, *FEBS Lett. 516*, 156−160.
12. Schulz, A., Ort, O., Beyer, P., and Kleinig, H. (1993) SC-0051, a 2-benzoyl-cyclohexane-1,3-dione bleaching herbicide, is a potent inhibitor of the enzyme *p*-hydroxyphenylpyruvate dioxygenase, *FEBS Lett. 318*, 162−166.
13. Lindstedt, S., and Rundgren, M. (1982) Blue color, metal content, and substrate binding in 4-hydroxyphenylpyruvate dioxygenase from *Pseudomonas* sp. strain P.J.874, *J. Biol. Chem. 257*, 11922−11931.
14. Rundgren, M. (1977) Steady-state kinetics of 4-hydroxyphenylpyruvate dioxygenase from human liver (III), *J. Biol. Chem. 252*, 5094−5099.
15. Johnson-Winters, K., Purpero, V. M., Kavana, M., Nelson, T., and Moran, G. R. (2003) (4-hydroxyphenyl)pyruvate dioxygenase from *Streptomyces avermitilis*: The basis of ordered substrate addition, *Biochemistry 42*, 2072−2080.
16. Choroba, O. W., Williams, D. H., and Spencer, J. B. (2000) Biosynthesis of the vancomycin group of antibiotics: Involvement of an unusual dioxygenase in the pathway to (*S*)-4-hydroxyphenylglycine, *J. Am. Chem. Soc. 122*, 5389−5390.
17. Gunsior, M., Ravel, J., Challis, G. L., and Townsend, C. A. (2004) Engineering *p*-hydroxyphenylpyruvate dioxygenase to a *p*-hydroxymandelate synthase and evidence for the proposed benzene oxide intermediate in homogentisate formation, *Biochemistry 43*, 663−674.
18. Lindblad, B., Lindstedt, G., and Lindstedt, S. (1970) The mechanism of enzymic formation of homogentisate from *p*-hydroxyphenylpyruvate, *J. Am. Chem. Soc. 92*, 7446−7449.
19. Serre, L., Sailland, A., Sy, D., Boudec, P., Rolland, A., Pebay-Peyroula, E., and Cohen-Addad, C. (1999) Crystal structure of *Pseudomonas fluorescens* 4-hydroxyphenylpyruvate dioxygenase: An enzyme involved in the tyrosine degradation pathway, *Structure 7*, 977−988.
20. Que, L., Jr. (2000) One motif—Many different reactions, *Nat. Stuct. Biol. 7*, 182−184.
21. Leinberger, R., Hull, W. E., Simon, H., and Retey, J. (1981) Steric course of the NIH shift in the enzymic formation of homogentisic acid, *Eur. J. Biochem. 117*, 311−318.
22. Rundgren, M. (1982) Tritium isotope effects in the reaction catalyzed by 4-hydroxyphenylpyruvate dioxygenase from *Pseudomonas* sp. strain P.J.874, *Biochim. Biophys. Acta 704*, 59−65.
23. Baldwin, J. E., Crouch, N. P., Fujishima, Y., Lee, M. H., MacKinnon, C. H., Pitt, J. P. N., and Willis, A. C. (1995) 4-hydroxyphenylpyruvate dioxygenase appears to display α-ketoisocaproate dioxygenase activity in rat liver, *Bioorg. Med. Chem. Lett. 5*, 1255−1260.
24. Adlington, R. M., Baldwin, J. E., Crouch, N. P., Lee, M. H., MacKinnon, C. H., and Paul, D. R. (1996) Stereochemistry of hydroxylation during the conversion of α-ketoisocaproate to *β*-hydroxyisovalerate by 4-hydroxyphenylpyruvate dioxygenase, *Bioorg. Med. Chem. Lett. 6*, 2721−2724.
25. Adlington, R. M., Baldwin, J. E., Crouch, N. P., Lee, M. H., and MacKinnon, C. H. (1996) Identification and stereochemistry of the product of 4-HPPD catalyzed oxidation of the ketoacid of methionine, *Bioorg. Med. Chem. Lett. 6*, 2003−2006.
26. Sono, M., Roach, M. P., Coulter, E. D., and Dawson, J. H. (1996) Heme-containing oxygenases, *Chem. Rev. 96*, 2841−2887.
27. Price, J. C., Barr, E. W., Tirupati, B., Bollinger, J. M., Jr., and Krebs, C. (2003) The first direct characterization of a high-valent iron intermediate in the reaction of an α-ketoglutarate-dependent dioxygenase: A high-spin Fe(IV) complex in taurine/α-ketoglutarate dioxygenase (TauD) from *Escherichia coli*, *Biochemistry 42*, 7497−7508.
28. Price, J. C., Barr, E. W., Glass, T. E., Krebs, C., and Bollinger, J. M., Jr. (2003) Evidence for hydrogen abstraction from C1 of taurine by high-spin Fe(IV) intermediate detected during oxygen activation by taurine:α-ketoglutarate dioxygenase (TauD), *J. Am. Chem. Soc. 125*, 13008−13009.
29. Proshlyakov, D. A., Henshaw, T. F., Monterosso, G. R., Ryle, M. J., and Hausinger, R. P. (2004) Direct detection of oxygen intermediates in the non-heme Fe enzyme taurine/α-ketoglutarate dioxygenase, *J. Am. Chem. Soc. 126*, 1022−1023.
30. Taniguchi, K., Kappe, T., and Armstrong, M. D. (1964) Further studied on phenylpyruvate oxidase, *J. Biol. Chem. 239*, 3389−3395.
31. Crouch, N. P., Adlington, R. M., Baldwin, J. E., Lee, M. H., and MacKinnon, C. H. (1997) A mechanistic rationalisation for the substrate specificity of recombinant mammalian 4-hydroxyphenylpyruvate dioxygenase (4-HPPD), *Tetrahedron 53*, 6993−7010.
32. Lin, Y. L., Huang, J. L., Wu, C. S., Liu, H. G., and Yang, D. Y. (2002) Design, synthesis, and evaluation of postulated transient intermediate and substrate analogues as inhibitors of 4-hydroxyphenylpyruvate dioxygenase, *Bioorg. Med. Chem. Lett. 12*, 1709−1713.
33. Becke, A. D. J. (1993) Density-functional thermochemistry. III. The role of exact exchange, *Chem. Phys. 98*, 5648−5652.
34. Lee, C., Yang, W., and Parr, R. G. (1988) Development of the Colle-Salvetti correlation energy formula into a functional of the electron density, *Phys. Rev. B 37*, 785−789.
35. Frisch, M. J., Trucks, G. W., Schlegel, H. B., Scuseria, G. E., Robb, M. A., Cheeseman, J. R., Zakrzewski, V. G., Montgomery, J. A., Jr., Stratmann, R. E., Burant, J. C., Dapprich, S., Millan, J. M., Daniels, A. D., Kudin, K. N., Strain, M. C., Farkas, O., Tomasi, J., Barone, V., Cossi, M., Cammi, R., Mennucci, B., Pomelli, C., Adamo, C., Clifford, S., Ochterski, J., Petersson, G. A., Ayala, P. Y., Cui, Q., Morokuma, K., Malick, D. K., Rabuck, A. D., Raghavachari, K., Foresman, J. B., Cioslowski, J., Ortiz, J. V., Stefanov, B. B., Liu, G., Liashenko, A., Piskorz, P., Komaromi, I., Gomperts, R., Martin, R. L., Fox, D. J., Keith, T., Al-Laham, M. A., Peng, C. Y., Nanayakkara, A., Gonzalez, C., Challacombe, M., Gill, P. M. W., Johnson, B., Chen, W., Wong, M. W., Andres, J. L., Head-Gordon, M., Replogle, E. S., and Pople, J. A. (1998) *GAUSSIAN98*, Gaussian Inc., Pittsburgh, PA.
36. *JAGUAR 4.0* (2000) Schrödinger, Inc., Portland, OR.
37. Tannor, D. J., Marten, B., Murphy, R., Friesner, R. A., Sitkoff, D., Nicholls, A., Ringnalda, M., Goddard, W. A., III, and Honig, B. (1994) Accurate first principles calculation of molecular charge distributions and solvation energies from ab initio quantum mechanics and continuum dielectric theory, *J. Am. Chem. Soc. 116*, 11875−11882.
38. Marten, B., Kim, K., Cortis, C., Friesner, R. A., Murphy, R., Ringnalda, M., Sitkoff, D., and Honig, B. (1996) New model for calculation of solvation free energies: Correction of self-consistent reaction field continuum dielelectric theory for short-range hydrogen-bonding effects, *J. Phys. Chem. 100*, 11775−11788.
39. Mouesca, J. M., Chen, J. L., Noodleman, L., Bashford, D., and Case, D. A. (1994) Density functional/Poisson-Boltzmann calculations of redox potentials for iron−sulfur clusters, *J. Am. Chem. Soc. 116*, 11898−11914.
40. Ciofini, I., and Daul, C. A. (2003) DFT calculations of molecular magnetic properties of coordination compounds, *Coord. Chem. Rev. 238* and *239*, 187−209.
41. Siegbahn, P. E. M., and Blomberg, M. R. A. (2000) Transition-metal systems in biochemistry studied by high-accuracy quantum chemical methods, *Chem. Rev. 100*, 421−437.
42. Blomberg, M. R. A., and Siegbahn, P. E. M. (2001) A quantum chemical approach to the study of reaction mechanisms of redox-active metalloenzymes, *J. Phys. Chem. B 105*, 9375−9386.
43. Siegbahn, P. E. M. (2003) Mechanisms of metalloenzymes studied by quantum chemical methods, *Q. Rev. Biophys. 36*, 91−145.
44. Borowski, T., Bassan, A., and Siegbahn, P. E. M. (2004) Mechanism of dioxygen activation in 2-oxoglutarate dependent enzymes. A hybrid DFT study, *Chem.—Eur. J. 10*, 1031−1041.
45. Ha, E. H., Ho, R. Y. N., Kisiel, J. F., and Valentine, J. S. (1995) Modeling the reactivity of α-ketoglutarate-dependent non-heme iron(II)-containing enzymes, *Inorg. Chem. 34*, 2265−2266.
46. Hegg, E. L., Ho, R. Y. N., and Que, L., Jr. (1999) Oxygen activation and arene hydroxylation by functional mimics of α-keto acid-dependent iron(II) dioxygenases, *J. Am. Chem. Soc. 121*, 1972−1973.
47. Bassan, A., Blomberg, M. R. A., and Siegbahn, P. E. M. (2003) Mechanism of dioxygen cleavage in tetrahydrobiopterin-dependent amino acid hydroxylases, *Chem.—Eur. J. 9*, 106−115.
48. Borowski, T., Bassan, A., and Siegbahn, P. E. M. (2004) A hybrid density functional study of O−O bond cleavage and phenyl ring hydroxylation for a biomimetic non-heme iron complex, *Inorg. Chem. 43*, 3277−3291.
49. Bassan, A., Blomberg, M. R. A., and Siegbahn, P. E. M. (2003) Mechanism of aromatic hydroxylation by an activated Fe^{IV}═O core in tetrahydrobiopterin-dependent hydroxylases, *Chem.—Eur. J. 9*, 4055−4067.

50. de Visser, S. P., Ogliaro, F., and Shaik, S. (2001) Stereospecific oxidation by compound I of cytochrome P450 does not proceed in a concerted synchronous manner, *Chem. Commun.* 2322−2323.
51. de Visser, S. P., and Shaik, S. (2003) A proton-shuttle mechanism mediated by the porphyrin in benzene hydroxylation by cytochrome P450 enzymes, *J. Am. Chem. Soc. 125*, 7413−7424.
52. Sevin, A., and Fontecave, M. (1986) Oxygen transfer from iron oxo porphyrins to ethylene. A semiempirical MO/VB approach, *J. Am. Chem. Soc. 108*, 3266−3272.
53. Zakharieva, O., Grodzicki, M., Trautwein, A. X., Veeger, C., and Rietjens, I. M. C. M. (1996) Molecular orbital study of the hydroxylation of benzene and monofluorobenzene catalysed by iron-oxo porphyrin π cation radical complexes, *J. Biol. Inorg. Chem. 1*, 192−204.
54. Zakharieva, O., Grodzicki, M., Trautwein, A. X., Veeger, C., and Rietjens, I. M. C. M. (1998) Molecular orbital study of porphyrin−substrate interactions in cytochrome P450 catalysed aromatic hydroxylation of substituted anilines, *Biophys. Chem. 73*, 189−203.
55. Moran, G. R., Derecskei-Kovacs, A., Hillas, P. J., and Fitzpatrick, P. F. (2000) On the catalytic mechanism of tryptophan hydroxylase, *J. Am. Chem. Soc. 122*, 4535−4541.
56. Hillas, P. J., and Fitzpatrick, P. F. (1996) A mechanism for hydroxylation by tyrosine hydroxylase based on partitioning of substituted phenylalanines, *Biochemistry 35*, 6969−6975.
57. Fitzpatrick, P. F. (1994) Kinetic isotope effects on hydroxylation of ring-deuterated phenylalanines by tyrosine hydroxylase provide evidence against partitioning of arene oxide intermediate, *J. Am. Chem. Soc. 116*, 1133−1134.
58. Jerina, D. M., Daly, J. W., and Witkop, B. (1968) The role of arene oxide-oxepin systems in the metabolism of aromatic substrates. II. Synthesis of 3,4-toluene-4-^{2}H oxide and subsequent "NIH shift" to 4-hydroxytoluene-3-^{2}H^{1}, *J. Am. Chem. Soc. 90*, 6523−6525.
59. Jerina, D. M., Daly, J. W., and Witkop, B. (1971) Migration of substituents during hydroxylation of aromatic substrates (NIH shift). Oxidations with peroxytrifluoroacetic acid, *Biochemistry 10*, 366−372.
60. Hocart, C. H., Halpern, B., Hick, L. A., and Wong, C. O. (1983) Hawkinsinuria−Dentification of quinolacetic acid and pyroglutamic acid during an acidotic phase, *J. Chromatogr., B 275*, 237−243.

BI049503Y